Mol Neurobiol (2015) 52:1637–1647
DOI 10.1007/s12035-014-8942-z

Role of Mitochondrial Calcium Uniporter in Early Brain Injury After Experimental Subarachnoid Hemorrhage

Huiying Yan · Dingding Zhang · Shuangying Hao · Kuanyu Li · Chun-Hua Hang

Received: 25 June 2014 / Accepted: 16 October 2014 / Published online: 5 November 2014

Abstract Previous studies have shown that mitochondrial Ca^{2+} is undertaken by mitochondrial calcium uniporter (MCU), and its accumulation is associated with the development of many diseases. However, little was known about the role of MCU in early brain injury (EBI) after subarachnoid hemorrhage (SAH). MCU can be opened by spermine under a physiological condition and inhibited by ruthenium red (RR). Herein, we investigated the effects of RR and spermine to reveal the role of MCU in SAH animal model. The data obtained with biochemical and histological assays showed that mitochondrial Ca^{2+} concentration was significantly increased in the temporal cortex of rats 1, 2, and 3 days after SAH, consistent with constant high levels of cellular Ca^{2+} concentration. In agreement with the observation in the acute phase, SAH rats showed an obvious increase of reactive oxygen species (ROS) level and decrease of ATP production. Blockage of MCU prevented Ca^{2+} accumulation, abated the level of oxidative stress, and improved the energy supply. Translocation of cytochrome c, increased cleaved caspase-3, and a large amount of apoptotic cells after SAH were reversed by RR administration. Surprisingly, exogenous spermine did not increase cellular Ca^{2+} concentration, but lessened the Ca^{2+} accumulation after SAH to benefit the rats. Taken together, our results demonstrated that blockage of MCU or prevention of Ca^{2+} accumulation after SAH is essential in EBI after SAH. These findings suggest that MCU is considered to be a therapeutic target for patients suffering from SAH.

Keywords Subarachnoid hemorrhage · Mitochondrial calcium uniporter · Early brain injury · Oxidative stress · Apoptosis

H. Yan · D. Zhang · C.-H. Hang (✉)
Department of Neurosurgery, Jinling Hospital, School of Medicine, Nanjing University, 305 East Zhongshan Road, Nanjing 210002, Jiangsu Province, China
e-mail: hang_neurosurgery@163.com

S. Hao · K. Li (✉)
Jiangsu Key Laboratory for Molecular Medicine, Medical School of Nanjing University, 22 Hankou Road, Nanjing 210093, Jiangsu Province, China
e-mail: likuanyu@nju.edu.cn

Introduction

Subarachnoid hemorrhage (SAH), a fatal subtype of stroke, accounts for only 5 % of all strokes. However, SAH mostly affects middle-aged patients with high disability and mortality rates, which, thus, imposes a heavy burden on society and economy [1, 2]. Early brain injury (EBI) and cerebral vasospasm are two major complications that often present in patients suffering from SAH. Past studies have focused primarily on cerebral vasospasm, and the reduction in angiographic vasospasm did not translate into a measurable clinical benefit in a clinical trial [3–5]. Recent studies have indicated that the pathophysiological event occurring within 72 h after SAH, as termed as EBI, is the most important factor determining the prognosis of patients suffering from SAH [6]. Various mechanisms have been attributed to the pathogenesis of EBI after SAH, including apoptosis, oxidative stress, and impaired calcium homeostasis [7].

Mitochondrial calcium uniporter (MCU) locates in the inner membrane of mitochondria. It can be inhibited by ruthenium red (RR) and opened by polyamine like spermine (Sper) [8, 9]. Under physiological conditions, mitochondrial Ca^{2+} uptake is undertaken by MCU. Imported mitochondrial Ca^{2+} can activate three matrix dehydrogenases, pyruvate dehydrogenase, isocitrate dehydrogenase, and α-ketoglutarate dehydrogenase. Stimulation of calcium-sensitive dehydrogenases, as a result, increases nicotinamide adenine dinucleotide hydrogen (NADH) availability and the flow of electrons down

the respiratory chain. Thus, adenosine triphosphate (ATP) synthesis is enhanced in the stimulated cells [10]. Under pathological conditions, mitochondrial Ca^{2+} overload is detrimental to mitochondrial function and can lead to electron leakage to increase reactive oxygen species (ROS) levels, further to directly damage the cells, known as apoptosis/necrosis [11]. Cellular and hence mitochondrial calcium accumulation, associated with increased ROS, mediate the sustained opening of mitochondrial permeability transition pore (mPTP). As a result, mitochondrial pro-apoptotic proteins, such as cytochrome c (cyt c) are released from the mitochondria to the cytoplasm [12–14]. Previous studies have shown that mitochondrial calcium accumulation is associated with the physiopathologic process of many diseases such as the ischemia/reperfusion injury of heart and brain [15, 16]. Rapid elevation in cytosolic free calcium was found after SAH, and treatment of nimodipine, a calcium channel blocker, can improve neurological outcomes but not cerebral vasospasm [7, 17]. The exact molecular mechanism of the role of calcium after SAH, however, has not been fully elucidated. The purpose of this study is to clarify the subcellular calcium accumulation and to investigate the potential role of MCU as a therapeutic target in EBI following SAH.

Methods and Materials

Animal Preparation

All procedures were approved by the Animal Care and Use Committee of Nanjing University and were conformed to Guide for the Care and Use of Laboratory Animals by National Institutes of Health. Male Sprague–Dawley (SD) rats (6–8 weeks, 270 to 330 g) were obtained from Animal Center of Jinling Hospital (Nanjing, China). The rats were housed in a humidity-controlled room (25±1 °C, 12-h light/dark cycle) and were raised with free access to water and food.

Experimental Design

Total 120 rats were randomly divided into the sham (surgery with normal saline insult, n=30), SAH (n=30), SAH+RR (SAH treated with RR 2.5 mg/kg, n=30), and SAH+Sper (SAH treated with Sper 5 mg/kg, n=30) groups. RR or Sper (both from Sigma, dissolved in sterile saline solution) were injected directly intraperitoneally (IP) at 15 min after SAH. The dose of 2.5 mg/kg RR and 5 mg/kg Sper was previously determined to be the optimal dosage for producing neuroprotective effects on ischemia/reperfusion injury in rats [16, 18]. No treatments were administered in the sham and SAH groups. Six rats from each group were selected randomly for the analysis of Western blot, cellular ATP and ROS analysis, cellular Ca^{2+} measurement, mitochondrial Ca^{2+} measurement, electron microscopic analysis, and immunofluorescence study at days 1, 2, and 3 after SAH. All counted rats were used for clinical evaluation including behavior examination and weighing.

Prechiasmatic Cistern Blood Injection for SAH Model

Experimental SAH models were performed as reported previously [19–21]. The rats were anesthetized with chloral hydrate (0.4 mg/kg, IP, Jinling Hospital). The hair on the head and near the inguinal region was carefully shaved, and then the rats were positioned prone in a stereotactic frame. After disinfection, a midline scalp incision was made and a 1-mm hole was drilled 8.0 mm anterior to the bregma in the midline of the skull, through the skull bone, down to duramater without perforating the underlying matter. Then, the animals were positioned supination. After disinfection again, we use insulin syringe (1 ml 29 G×1/2 m, 0.33 mm×12.7 mm) (BD Science) to draw 300-μl volume of blood from femoral artery. The needle was advanced 11 mm into the prechiasmatic cistern through the burr hole, at a 45° angle to the vertical plane, and the 300 μl of blood was injected into the prechiasmatic cistern over 20 s. Loss of cerebrospinal fluid (CSF) and bleeding from the midline vessels were prevented by plugging the burr hole with bone wax prior to inserting the needle. Sham animals were injected with 300 μl normal saline. After injection, animals were kept in a 30 °C, heads-down position for 20 min. After recovery from anesthesia, the rats were returned to their cages and housed at 25±1 °C. Rats that died during surgery or during surgical recovery were excluded, and the procedure was repeated until final group sizes reached the planned experimental number.

Clinical Evaluation

Three behavioral activity examinations were performed at day 2 after SAH using the previously described scoring system modified for rodent subjects [22]. Scoring was conducted by two independent researchers blinded to the groups. Grading of neurologic deficits was as follows: 1, no neurologic deficit (scores=0); 2, minimum or suspicious neurologic deficit (scores=1); 3, mild neurologic deficit (scores=2–3); and 4, severe neurologic deficit (scores=4–6). Appetite was qualified by body weight change. The rats of each group were weighed at days 1, 2, and 3 after drug injection, and body weight change was calculated as follows:

$$\text{Body weight change} = \text{body weight at indicated time after injection} - \text{body weight 15 min before injection}$$

Perfusion–Fixation and Tissue Preparation

Animals were anesthetized as above and perfused through the left cardiac ventricle with normal saline (4 °C) until effluent from the right atrium was clear. Animals which had obvious clots in the prechiasmatic cistern were selected for further analysis. The temporal lobe tissue (Fig. 1b) which was near the hematoma was harvested on ice after blood clots on the tissue cleared carefully. The fresh tissues were used for cellular ROS/ATP analysis and mitochondria isolation. The other tissues were stored in −80 °C till further use for Western blot and measurement of cellular Ca^{2+}. For immunofluorescence study, the rats were perfused with normal saline (4 °C), followed by 4 % buffered paraformaldehyde (4 °C), and then the brains were immersed in 4 % buffered paraformaldehyde (4 °C) for further study.

Isolation of Mitochondria

A tissue mitochondria isolation kit (Beyotime, China) was used to isolate mitochondria and cytoplasmic fraction. The mitochondria from fresh tissues were lysed for measurement of mitochondrial Ca^{2+} and mitochondrial protein extraction. The cytoplasmic and mitochondrial proteins were stored in −80 °C for Western blot analysis.

Measurement of Cellular and Mitochondrial Ca^{2+} Levels

Measurement of cellular and mitochondrial Ca^{2+} levels were conducted with a tissue Ca^{2+} concentration quantitative determination kit (Genmed Scientifics Inc.) and a mitochondrial Ca^{2+} concentration quantitative determination kit (Genmed Scientifics Inc.) according to the instruction from the manufacturer.

Measurement of Cellular ATP and ROS Levels

Cellular ATP levels were measured using a firefly luciferase-based ATP assay kit (Beyotime), and cellular ROS levels were analyzed using a ROS assay kit based on a fluorescence technique (Genmed Scientifics Inc.) according to the given protocol.

Western Blot Analysis

Western blot analysis was conducted as previously described [23]. Briefly, cerebral tissues were completely homogenized using lysis buffer (Thermo Fisher Scientific), followed by centrifugation at 14,000×*g* for 15 min at 4 °C. The supernatant was collected as the total protein extraction. Protein concentration was determined with a BCA kit (Beyotime), and proteins were normalized to 15 μg per lane for mitochondrial cytochrome c (mito-cyt c) analysis, 30 μg per lane for total/cytoplasmic cytochrome c (cyto-cyt c) analysis, and 70 μg per lane for cleaved caspase-3 analysis. For Western blot analysis, an equal volume of 2× sodium dodecyl sulfate (SDS) sample loading buffer was added to the protein extraction, and the samples were then boiled for 5 min. Then, the samples were subjected to electrophoresis on 15 % SDS polyacrylamide gels for 30 min at 80 V, followed by 100 min at 100 V and then transferred onto nitrocellulose membrane (NC, PALL) sheets for 90 min at 250 mA. After blocked with 5 % skim milk for 90 min at room temperature, the sheets were incubated with primary antibodies at 4 °C overnight. Anti-cyt c (1:5,000 dilution, Abcam, UK), anti-cleaved caspase-3 (1:500 dilution, Cell Signaling Technology, USA), anti-β-tubulin (1:1,000 dilution, Sigma), and anti-VDAC (1:1,000 dilution, Cell Signaling Technology) were used in this study. Then, the membranes were washed with Tween 20 in Tris-buffered saline (TTBS, 100 mM Tris–HCl, pH 7.5, 0.9 % NaCl, 0.1 % Tween 20). After incubation with secondary antibodies and washing again, the blotted protein bands were

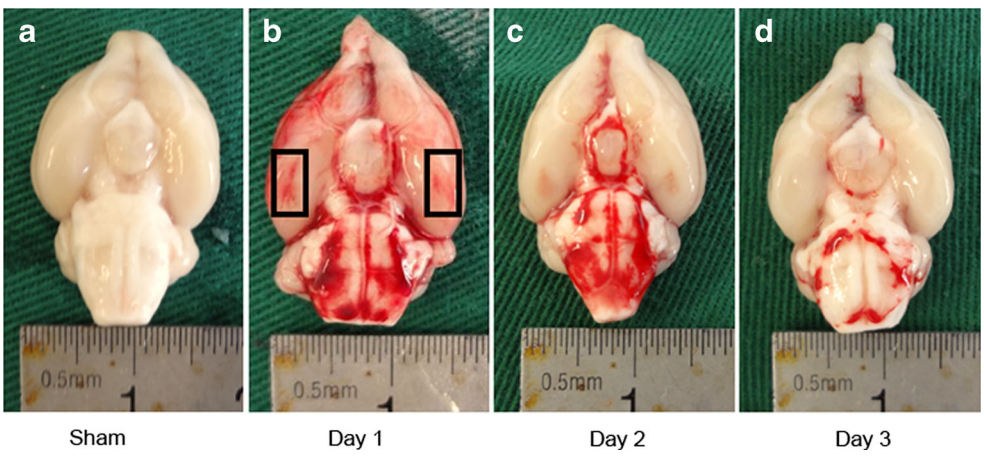

Fig. 1 Schematic representatives of the brains for sham group (**a**) and SAH group at day 1 (**b**), day 2 (**c**), and day 3 (**d**). The areas taken for assays in this study were shown in *black boxes* for all samples. Bloody clots in the subarachnoid space rapidly disappeared within 3 days

visualized by enhanced chemiluminescence Western blot detection reagents (Thermo Fisher Scientific). Relative changes in protein expression were estimated from the mean pixel density using UN-SCAN-IT, normalized to β-tubulin (VDAC for mitochondrial protein), and calculated as target protein expression/β-tubulin (VDAC) expression ratios.

Identification of Brain Mitochondria Using Electron Microscopy

At day 2 after SAH, the rats were killed as above and perfused with 2.5 % buffered glutaraldehyde. The temporal lobe tissues were immediately fixed with 2.5 % buffered glutaraldehyde for 3 h. The specimens were then minced into smaller (<1 mm^3) fragments and again fixed with glutaraldehyde for 1 h, postfixed with 1 % OsO_4 in the same buffer for 1 h, dehydrated with alcohol, and embedded in araldite. Semi-thin sections were prepared, stained with 1 % toluidine blue in distilled water at 60 °C, and observed by light microscopy. The semi-thin sections were trimmed over the neurons in order to have an overview of the mitochondria in neurons. For ultrastructural analysis, nickel grids were used as supports. Thin sections, stained with uranyl acetate and lead citrate, were observed with a transmission electron microscope JEM-1011 (JEOL, Japan).

Terminal Deoxynucleotidyl Transferase (TdT) dUTP Nick-End Labeling (TUNEL) Staining

Brain tissues fixed with 4 % paraformaldehyde were dipped in 20 % saccharose phosphate-buffered saline (PBS) for 2 days and then in 30 % saccharose PBS for another 2 days to remove water in the tissues. Sections 7 μm in thickness were sliced and washed with PBS. TUNEL assay was conducted using an In Situ Cell Death Detection Kit (Roche Inc., Indianapolis, USA) just as the given protocol. Then, the sections were counterstained by 4′, 6-diamidino-2-phenylindole (DAPI, Beyotime) for 3 min. After three washes again, the slides were covered by microscopic glass with Antifade Mounting Medium (Beyotime) for further study. Fluorescence microscopy imaging was performed using ZEISS HB050 inverted microscope system (Zeiss, German). The positive cells were identified, counted, and analyzed by two investigators blinded to the grouping. The extent of brain damage was evaluated by the apoptotic index, defined as the average percentage of TUNEL-positive cells in each section counted in six cortical microscopic fields (at ×400 magnification). Four animals per group were analyzed.

Nissl Staining and Cell Counting

For Nissl staining, the 4-μm sections were hydrated in 1 % toluidine blue at 50 °C for 20 min. After rinsing with double-distilled water, the sections were dehydrated and mounted with permount. Normal neurons have relatively big cell body, rich in cytoplasm, with one or two big round nuclei, while damaged cells show shrunken cell bodies, condensed nuclei, dark cytoplasm, and many empty vesicles. Cell counting was restricted to the temporal lobe. Six random high-power fields (400×) in each coronary section were chosen, and the mean number of surviving neurons in the six views was regarded as the data of each section. A total of four sections from each animal were used for quantification. The final average number of the four sections was regarded as the data for each sample. Data were presented as the number of neurons per high-power field. All the processes were conducted by two pathologists blinded to the grouping.

Statistical Analysis

All data were presented as mean±SD. SPSS 17.0 was used for statistical analysis of the data. All data were subjected to one-way ANOVA. Differences between experimental groups were determined by the Fisher's LSD posttest. Statistical significance was inferred at $P<0.05$.

Results

RR and Sper Improved the Appetite of SAH Rats and Helped Rats Gain Weight

The SAH model of rats was established well in this study. Among all the experimental animals ($n=136$), 106 rats were injected with blood, 16 of which (15.1 %) died while no animals died in the sham group ($n=30$). All mortality occurred within 48 h of surgery and mortality rates were not significantly different among the SAH, SAH+RR, and SAH+Sper groups (data not shown). Four rats with SAH were excluded later from the study because of little blood in prechiasmatic cistern but lots of blood clot in the frontal lobe instead. The blood clots could easily be found on surface of temporal lobe and around the basilar arteries in SAH rats (Fig. 1b), while there was no visible blood in sham rats (Fig. 1a). It was also demonstrated that the blood clot in subarachnoid space disappeared rapidly within 72 h after blood injection (Fig. 1b–d).

Among the experimental groups, we hardly found obvious neurological deficits including movement and reaction to stimulation. However, marked change of appetite was observed in all injection rats, displaying less food to eat and water to drink. Consequently, body weight of the rats got lost (Fig. 2). There was no significant difference of body weight change at day 1 among the SAH, SAH+RR, and SAH+Sper groups. The SAH rats treated with RR showed less loss of body weight at day 2 and day 3 than SAH-only group. Surprisingly, the SAH rats treated with Sper also presented

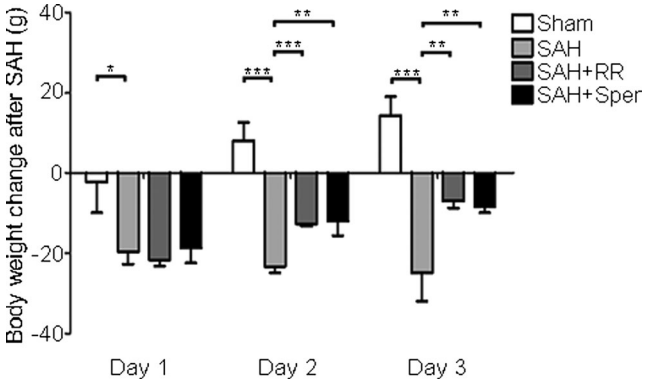

Fig. 2 The changes of body weight after SAH. The body weight of the rats in the SAH group remarkably reduced compared with the sham group. There was no significant difference of the body weight between SAH, SAH+RR, and SAH+Sper groups at day 1. At days 2 and 3, treatment with RR and Sper could obviously alleviate the loss of body weight. *Bars* represent the mean±SD (n=5 in each group). *P<0.05, **P<0.01, ***P<0.001. For the definitions of SAH, SAH+RR, and SAH+Sper groups, see the "Methods and Materials" section

less loss of body weight at day 2 and day 3 than the SAH group (Fig. 2).

SAH Increased Both Cellular and Mitochondrial Ca^{2+} Concentrations, and RR and Sper Prevented the Effects

Calcium homeostasis is essential for physiological cell function, and impaired calcium homeostasis is involved in the development of brain injury after SAH [7]. In the present study, both cellular and mitochondrial Ca^{2+} concentrations of temporal cortex were measured. The results showed that both cellular and mitochondrial Ca^{2+} concentrations increased significantly in the SAH group, and the levels were kept constantly high within 3 days, particularly in mitochondria (Fig. 3, P<0.05). Nevertheless, treatment with RR markedly reduced cellular and mitochondrial Ca^{2+} concentrations (P<0.05). Surprisingly and consistently, cellular and mitochondrial Ca^{2+} concentrations in SAH rats treated with Sper also decreased remarkably (P<0.05). Combined with the gain-of-weight effect of Sper on SAH rats, this result suggested that Sper could inhibit MCU or prevent Ca^{2+} accumulation to protect from EBI.

SAH Triggered the Elevated ROS Levels and Limited Mitochondrial ATP Generation

As much as Ca^{2+} signaling is altered in the injured cells, excess ROS can be produced due to an ineffective coupling of mitochondrial respiration. To observe whether ROS generation after SAH is affected by mitochondrial Ca^{2+} overload, ROS levels were monitored by detection of 2′,7′-dihydrodichlorofluorescein diacetate (DCFH-DA) fluorescence. In the sham group, low levels of DCFH-DA fluorescence were observed. There was a marked increase of

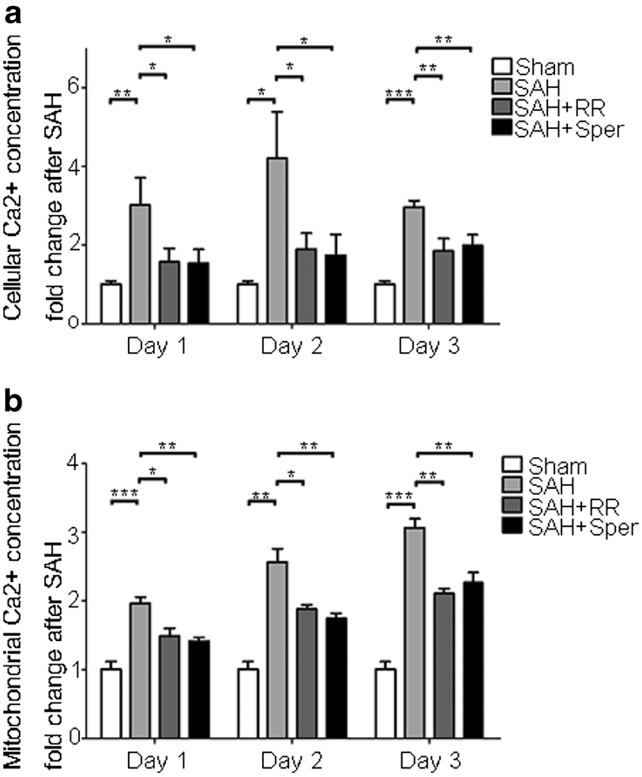

Fig. 3 Restored cellular (**a**) and mitochondrial (**b**) concentrations of Ca^{2+} by RR or Sper treatment after SAH. *Bars* represent the mean±SD (n=5 in each group). *P<0.05, **P<0.01, ***P<0.001. Definition of SAH, SAH+RR, and SAH+Sper groups is the same as in Fig. 2

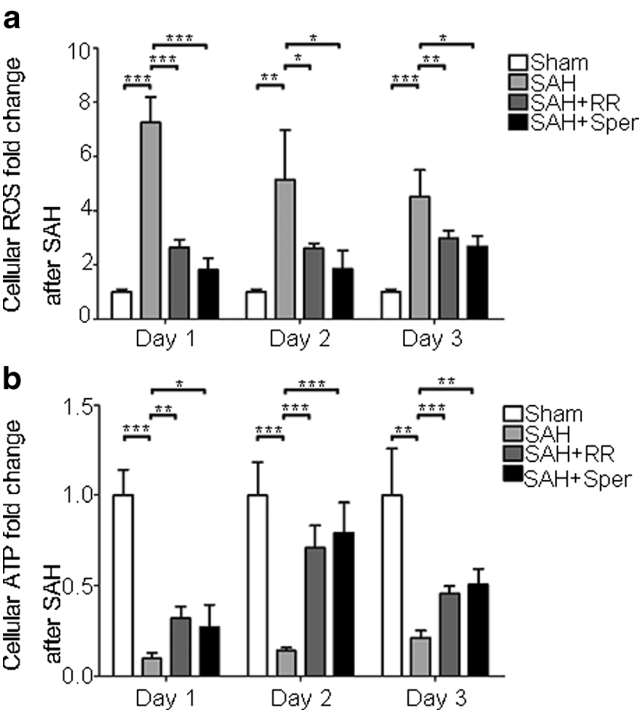

Fig. 4 Reversed cellular ROS (**a**) and ATP (**b**) levels by RR or Sper treatment after SAH. **a** Cellular ROS levels after SAH were repressed by RR or Sper administration. **b** Cellular ATP was resupplied after SAH by RR or Sper administration. *Bars* represent the mean±SD (n=5 in each group). *P<0.05, **P<0.01, ***P<0.001

fluorescence in the SAH group ($P<0.05$), reaching a maximum at day 1 and then declining at day 2 and day 3 (Fig. 4a), indicative of a rapid increase of ROS production. Following treatment with RR and Sper, ROS generation was observed to be significantly less than the sham group ($P<0.05$).

Calcium homeostasis depends on adequate supply of ATP for maintaining ionic gradients across the cell membrane. Overload calcium may be involved in the insufficient ATP supply. As shown in Fig. 4b, ATP levels in SAH rats dramatically decreased, compared with sham group ($P<0.05$). Treatment with RR or Sper rescued the ATP supply fundamentally ($P<0.05$) at day 2. We speculate that a single dose of RR or Sper had a transient neuroprotective effect which is very important in EBI.

SAH Deformed the Mitochondria, and RR and Sper Stabilized Them

Mitochondrial calcium accumulation, associated with increased ROS and insufficient ATP supply, mediates the sustained opening of mPTP, as a result, leading to mitochondria swelling even break [24]. To investigate the possible mitochondrial damage in EBI after SAH, electron microscopy was used. In the sham group, mitochondria were revealed to have intact membranes, regular cristae, and dense matrix space under electron microscopy (Fig. 5a). The swelling shape, disruption of the membranes, and near disappearance of the cristae were evident after SAH (Fig. 5b). Treatment with RR and Sper could obviously protect the mitochondria from deformation (Fig. 5c, d).

SAH Induced Apoptosis, and RR and Sper Blocked the Effect

To provide the molecular evidence of mitochondrial damage after SAH, other than the morphological severe change, we determined the translocation of cyt c, which is released from the intermembrane space of mitochondria to cytosol due to the opening of mPTP. Subcellular fractionation and Western blot were used to detect the levels of cyt c in mitochondria and cytosol, respectively. The results showed that SAH promoted a marked release of cyt c from mitochondria (Fig. 6a, b, $P<0.05$), therefore increased the level in cytoplasm (Fig. 6c, d, $P<0.05$), reaching a maximum at day 2 after SAH, while no clear change of total cyt c ($P>0.05$) was found (Fig. 6e, f). Treatment with RR and Sper greatly increased mito-cyt c levels and decreased cyto-cyt c levels ($P<0.05$), compared with SAH group.

Release of cyt c from injured mitochondria into the cytosol may initiate apoptosis. Caspase-3 can, in turn, be activated, which is an important indicator of apoptosis [25–27]. We then analyzed whether the activation of caspase-3 was coupled with the release of cyt c with Western blotting by evaluating

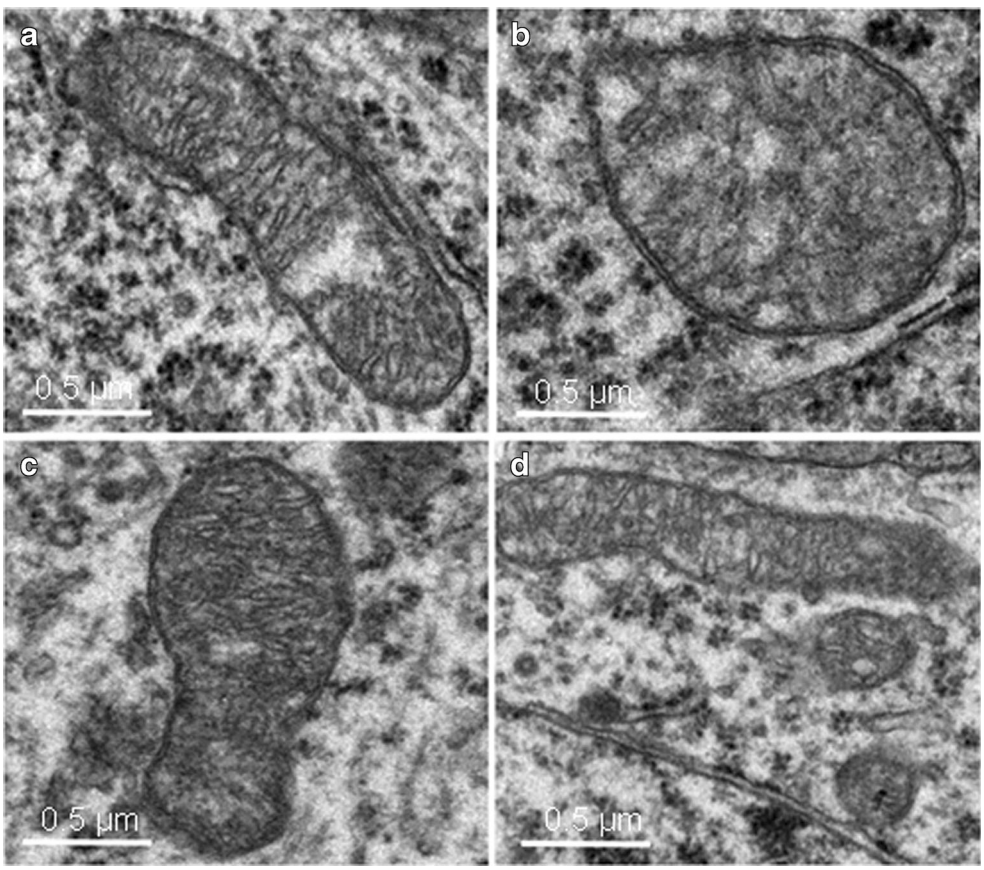

Fig. 5 Electron photomicrographs of mitochondria after SAH. A representative of a mitochondrion with normal shape from the cortex of the sham group (**a**), a swelling mitochondrion with collapsed cristae from the cortex of the SAH group (**b**), a mitochondrion with quite normal shape from the cortex of the SAH+RR group (**c**), and mitochondria with clear cristae from the cortex of the SAH+Sper group (**d**). *Scale bar* indicates 0.5 μm

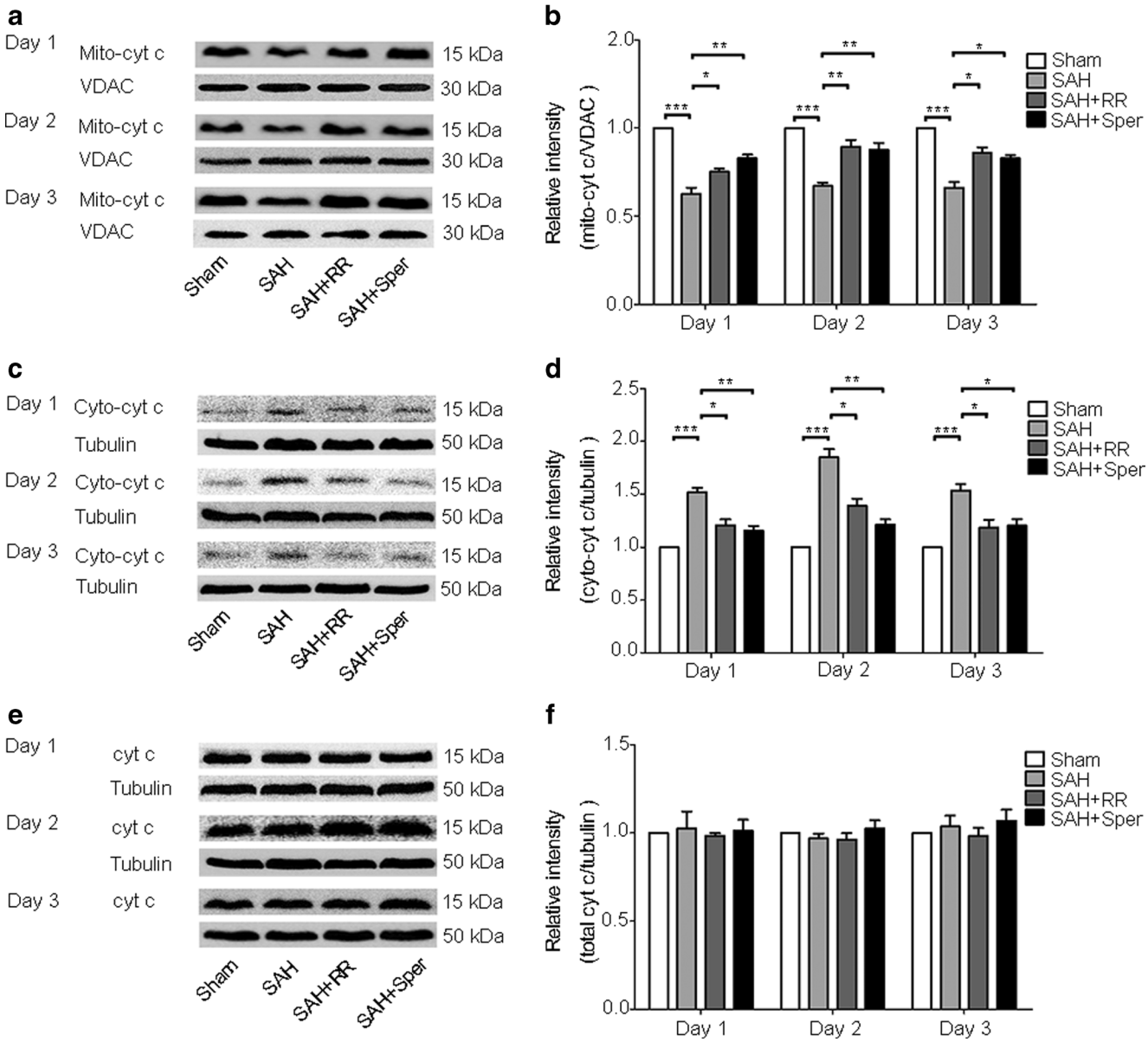

Fig. 6 Translocation of cytochrome c after SAH and protective effects of RR and Sper. Representative Western blots to show cytochrome c levels in mitochondria (**a**), cytoplasm (**c**), and cells in total (**e**). **b**, **d**, and **f** are quantitative data from **a**, **c**, and **e**, respectively. As shown here, mitochondrial cytochrome c release took place after SAH and was significantly inhibited by RR and Sper treatment, while the levels of the total cellular cytochrome c were kept constant. *Bars* represent the mean±SD (n=5 in each group). *P<0.05, **P<0.01, ***P<0.001

cleaved caspase-3 level. Cleaved caspase-3 production increased obviously after SAH (P<0.05) compared to sham group, reaching a maximum at day 2 (Fig. 7). This increase after SAH was markedly attenuated to a great extent by systemic administration with RR or Sper (Fig. 7a, b, P<0.05).

To further analyze the SAH-induced apoptosis and effect of the two drugs, TUNEL assay was designed to detect apoptotic cells that undergo extensive DNA degradation during the late stages of apoptosis with the cortex samples at day 2 after SAH. In the sham group, few TUNEL-positive cells were found (Fig. 8a, e, i). However, numerous TUNEL-positive cells with chromatin condensation and fragmented nuclei could be easily found in the temporal cortex (Fig. 8b, f, j, P<0.001), which was positively correlated with the levels of released cyt c from mitochondria and cleaved caspase-3. Treatment with RR (Fig. 8c, g, k, P<0.01) or Sper (Fig. 8d, h, l, P<0.01) triggered a significant reduction in TUNEL-positive cells compared with the SAH animals.

The Number of the Neurons Reduced After SAH and Reversed by RR and Sper Treatment

The induced apoptosis in the early response to SAH would cause neurons' death. To confirm this, Nissl staining was

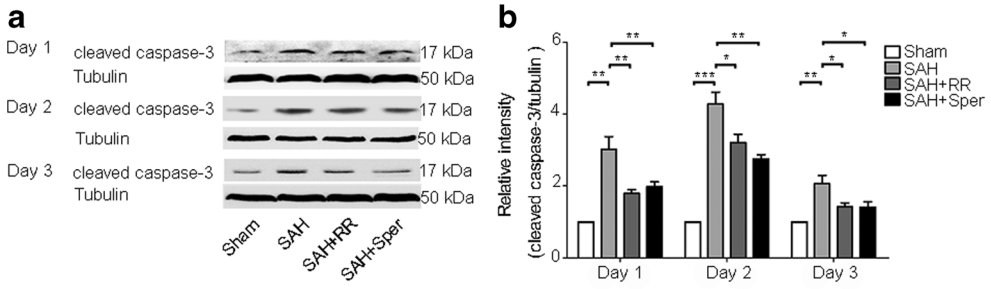

Fig. 7 Activation of caspase-3 after SAH and prevention of RR and Sper from the cleavage. **a** Representative autoradiogram of the increased cleaved caspase-3 after SAH and prevention by RR and Sper from cleavage, revealed with Western blots. **b** Quantitative data of cleaved caspase-3. *Bars* represent the mean±SD (n=5 in each group). *P<0.05, **P<0.01, ***P<0.001

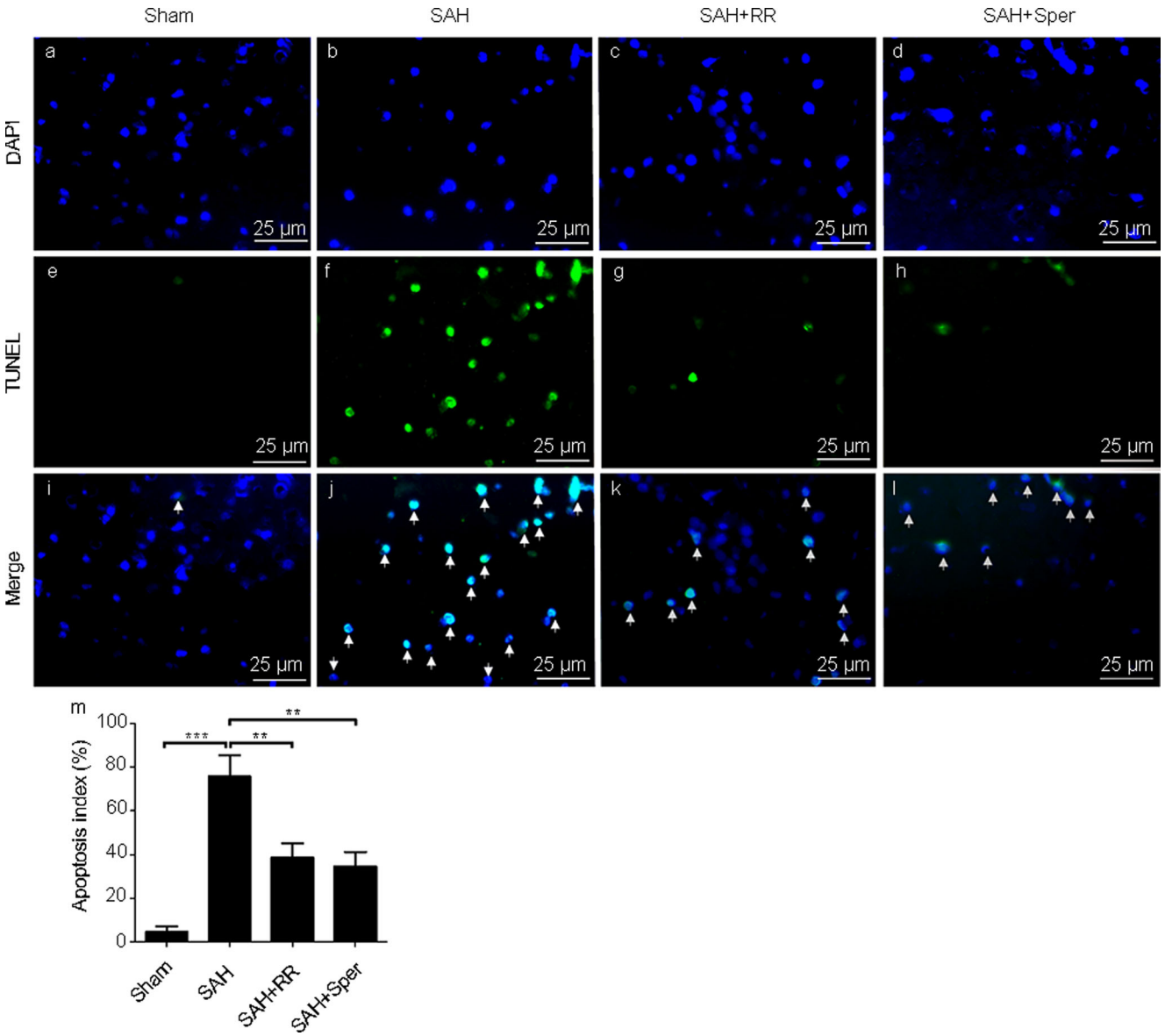

Fig. 8 Apoptotic cells triggered by SAH and prevented by RR and Sper, revealed by TUNEL staining of the brain slices. Representative micrographs of DAPI-positive (**a**–**d**, **i**–**l**) and TUNEL-positive (**e**–**h**, **i**–**l**) stained cells in the temporal cortex. **m** Apoptosis index of the slides with TUNEL staining. *Bars* represent the mean±SD (n=5 in each group). **P<0.01, ***P<0.001. *Scale bar* indicates 25 μm

applied to illustrate the number and morphology change of the remained neurons in the cortex. In the sham group, rare injured neurons were detected (Fig. 9a, e). The visual field was full of clear and intact neurons, without edema around the cells. While a significant proportion of neurons in the SAH group were damaged (Fig. 9b, f, $P<0.01$), exhibiting extensive degenerative changes including sparse cell arrangements, loss of integrity, shrunken cytoplasma, oval or triangular nucleus, and swollen cell bodies. In contrast, the severity of neuronal degeneration in the SAH+RR (Fig. 9c, g, $P<0.01$) and SAH+Sper (Fig. 9d, h, $P<0.01$) groups was evidently alleviated compared to that in the SAH group.

Discussion

The present study provides evidence that intraperitoneal administration of RR could reverse the injury resulting from SAH to a great extent during the early phase. More notably, Sper, thought to be an opener of MCU for calcium access to mitochondria, showed a similar effect to RR, a blocker of MCU. Interestingly, the molecular mechanism of the neuroprotective effect of both RR and Sper from SAH is, likely, through inhibiting MCU to decrease the levels of mitochondrial and cellular calcium accumulation.

Calcium is crucial as a second messenger in modulating many cellular physiological functions, but Ca^{2+} overload is detrimental to mitochondria. Mitochondrial dysfunction that is caused by excessive Ca^{2+} uptake through the MCU is a key event in severe excitotoxicity that leads to depolarization of $\Delta\psi m$, ROS generation, and inhibition of ATP production. Our results supported that Ca^{2+} overload coupled the stimulated ROS generation due to the defects in mitochondrial energy metabolism. An increase in ROS can also modulate Ca^{2+} dynamics and augment Ca^{2+} surge [28]. The reciprocal interactions between Ca^{2+}-induced ROS increase and ROS modulated Ca^{2+} upsurge may cause a feed forward, self-amplified loop that creates cellular damage

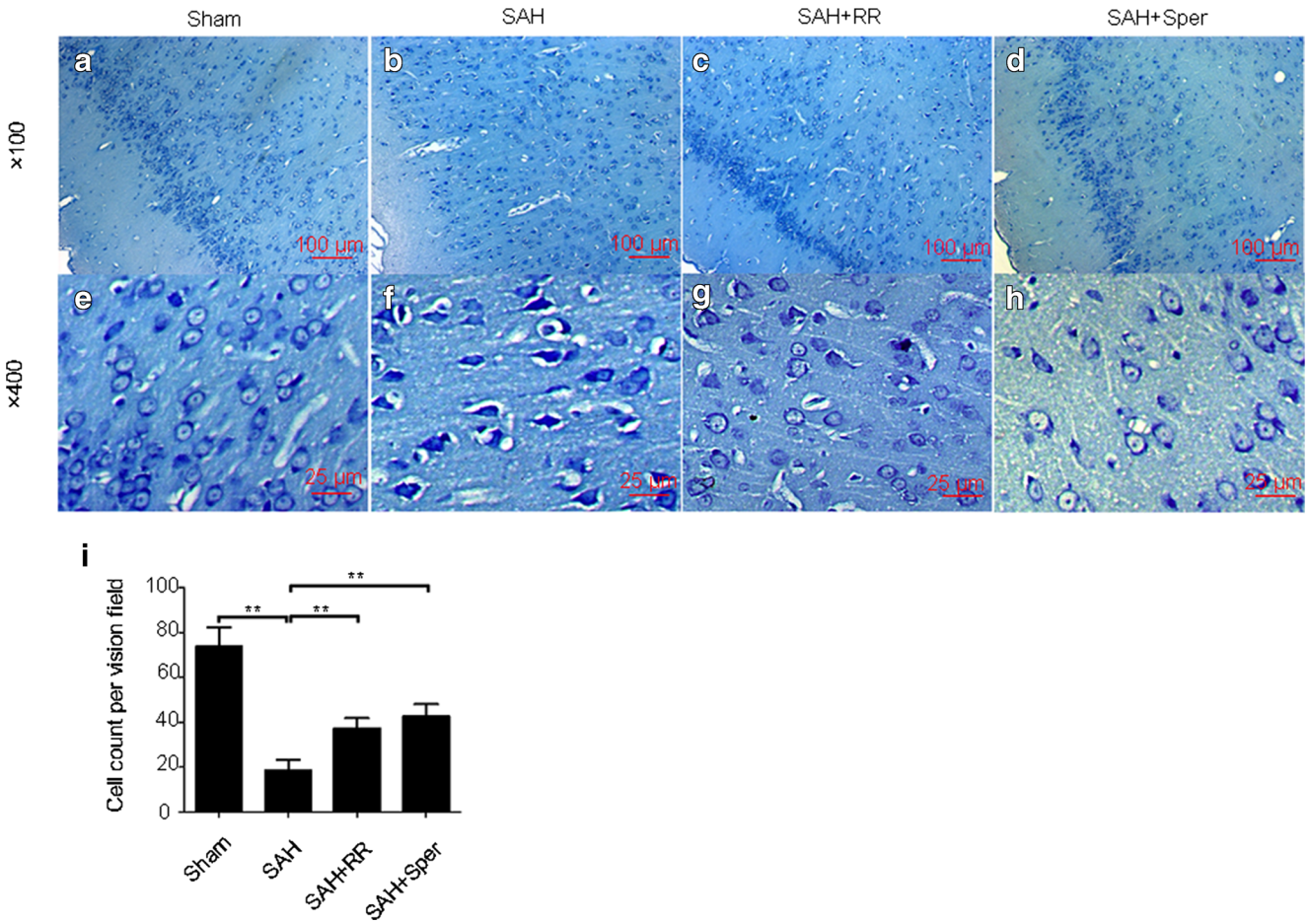

Fig. 9 Nissl staining to visualize the neuronal cell outline and structure. SAH reduced the number of the neurons, and treatment of RR or Sper preserved neurons from damage, including neuron loss and degeneration. SAH group (**b**, **f**): cells were arranged sparsely, and the cell outline was fuzzy, compared with sham group (**a**, **e**). Groups SAH+RR (**c**, **g**) and SAH+Sper (**d**, **h**): drugs substantially increased the proportion of survived neurons. **i** Cell counts per visual field (×400) was quantified in the slides with Nissl staining. Representative slides of Nissl staining at two different magnifications (**a**–**d**, ×100; **e**–**h**, ×400). *Bars* represent the mean±SD ($n=5$ in each group). $^{**}P<0.01$

far beyond direct Ca^{2+}-induced damage [11]. As observed in this study, blockage of MCU could remarkably alleviate this overload. As a result, ROS production was decreased and the energy supply of the brain was improved. Consequently, RR and Sper protected the neurons from injury, which is very important for a long-term neurological improvement suffering from SAH.

The maintenance of mitochondrial Ca^{2+} homeostasis in neurons is modulated by MCU, which locates in the inner membrane of mitochondria. It can rapidly transport cytoplasmic Ca^{2+} into the mitochondrial matrix, driven by the negative charge of the membrane potential established by the respiratory chain [29]. In consistence with previous reports, we showed that SAH caused cytosolic and mitochondrial Ca^{2+} overload, which is an essential event to initiate cell death [30]. As anticipated, treatment of RR after SAH abated the Ca^{2+} uptake/accumulation and level of oxidative stress, further improved the energy supply. The unexpected protective effect of Sper differs from other studies [16, 18, 31, 32], although Sper was proposed as an antioxidant to scavenge hydroxyl radicals at physiological concentrations [33]. The properties of antioxidant and pro-oxidant activities of Sper depend on what conditions the cells are under [34]. Under oxidizing condition, especially in the presence of iron and copper ions, Sper acts as an oxidant, which phenomenon is well known for ascorbic acid [34, 35]. Thus, Sper is not a simple activator of MCU to stimulate Ca^{2+} uptake. Even though, Sper may be bidirectionally transported across the inner membrane by cycling, in which influx and efflux are driven by electrical and pH gradients, respectively [36]. SAH-induced mitochondrial injury could make the membrane at least partial permeable, which would cause a movement of ions down the concentration gradient. As a result, Sper cycling stops, which may unfavor the Ca^{2+} accumulation in the mitochondria to have a protective effect as observed in this study.

A substantial amount of evidence indicates that brain injury begins at the aneurysm rupture, and rapid Ca^{2+} influx was observed in several studies and is involved in the pathophysiological process of brain injury [30, 37, 38]. If the EBI after SAH could be blocked, the patient's outcome would be markedly improved [7, 39]. Due to the early nature, drugs were administrated within 15 min after SAH in this animal model of EBI. Within 3 days, the substantial improvement of the effects of SAH from the administration of RR and Sper was observed in all aspects including ROS levels, apoptosis, neuronal death, and weight loss of the animals. Thus, the failure of clinical translation of therapies, very likely, results from no prompt interference with the calcium/ROS levels.

We have proven in present study that blockage of MCU has beneficial effects in attenuating EBI. It is still not clear that a single dose of RR or Sper may not provide long-lasting protection. In the future, we will use different dosages and time windows of medicine taken and method of administration to test whether blockage of MCU could improve the long-term outcome after SAH.

Summary

In the acute phase after SAH, mitochondrial calcium overload may produce a large amount of ROS and lead to cellular bioenergetic crisis, which in turn contributed to cell death. Blockage of MCU or prevention of Ca^{2+} accumulation could significantly ameliorate oxidative injury and reduce neuronal cell death. Thus, MCU may be a potential therapeutic target for patients suffering from SAH.

Acknowledgments We would like to thank Dr. Chunxi Wang, Guangbin Xie, and Yuqiu Lu for their technical assistance. This study was supported by the National Natural Science Foundation, China (nos. 81371294, 31071085, and 31371060).

References

1. Green DM, Burns JD, DeFusco CM (2013) ICU management of aneurysmal subarachnoid hemorrhage. J Intensive Care Med 28:341–354
2. American Heart Association Stroke C, Council on Cardiovascular R, Intervention, Council on Cardiovascular N, Council on Cardiovascular S, Anesthesia, Council on Clinical C, Connolly ES Jr, Rabinstein AA, Carhuapoma JR, Derdeyn CP, Dion J, Higashida RT, Hoh BL, Kirkness CJ, Naidech AM, Ogilvy CS, Patel AB, Thompson BG, Vespa P (2012) Guidelines for the management of aneurysmal subarachnoid hemorrhage: a guideline for healthcare professionals from the American Heart Association/American Stroke Association. Stroke 43:1711–1737
3. Topkoru BC, Altay O, Duris K, Krafft PR, Yan J, Zhang JH (2013) Nasal administration of recombinant osteopontin attenuates early brain injury after subarachnoid hemorrhage. Stroke 44:3189–3194
4. Macdonald RL, Higashida RT, Keller E, Mayer SA, Molyneux A, Raabe A, Vajkoczy P, Wanke I, Bach D, Frey A, Marr A, Roux S, Kassell N (2011) Clazosentan, an endothelin receptor antagonist, in patients with aneurysmal subarachnoid haemorrhage undergoing surgical clipping: a randomised, double-blind, placebo-controlled phase 3 trial (CONSCIOUS-2). Lancet Neurol 10:618–625
5. Vergouwen MD, Ilodigwe D, Macdonald RL (2011) Cerebral infarction after subarachnoid hemorrhage contributes to poor outcome by vasospasm-dependent and -independent effects. Stroke 42:924–929
6. Cahill J, Zhang JH (2009) Subarachnoid hemorrhage: is it time for a new direction? Stroke 40:S86–S87
7. Sehba FA, Hou J, Pluta RM, Zhang JH (2012) The importance of early brain injury after subarachnoid hemorrhage. Prog Neurobiol 97:14–37
8. Nicchitta CV, Williamson JR (1984) Spermine. A regulator of mitochondrial calcium cycling. J Biol Chem 259:12978–12983
9. Kirichok Y, Krapivinsky G, Clapham DE (2004) The mitochondrial calcium uniporter is a highly selective ion channel. Nature 427:360–364
10. McCormack JG, Halestrap AP, Denton RM (1990) Role of calcium ions in regulation of mammalian intramitochondrial metabolism. Physiol Rev 70:391–425

11. Peng TI, Jou MJ (2010) Oxidative stress caused by mitochondrial calcium overload. Ann N Y Acad Sci 1201:183–188
12. Di Lisa F, Bernardi P (2009) A CaPful of mechanisms regulating the mitochondrial permeability transition. J Mol Cell Cardiol 46:775–780
13. Owens K, Park JH, Schuh R, Kristian T (2013) Mitochondrial dysfunction and NAD(+) metabolism alterations in the pathophysiology of acute brain injury. Transl Stroke Res 4:618–634
14. O'Rourke B (2000) Pathophysiological and protective roles of mitochondrial ion channels. J Physiol 529:23–36
15. Orrenius S, Zhivotovsky B, Nicotera P (2003) Regulation of cell death: the calcium-apoptosis link. Nat Rev Mol Cell Biol 4:552–565
16. Zhao QW, Li S, Wang Y, Li P, Guo S, Yao YR (2013) The role of the mitochondrial calcium uniporter in cerebral ischemia/reperfusion injury in rats involves regulation of mitochondrial energy metabolism. Mol Med Rep 7:1073–1080
17. American Heart Association Stroke C, Council on Cardiovascular R, Intervention, Council on Cardiovascular N, Council on Cardiovascular S, Anesthesia, Council on Clinical C, Connolly ES Jr, Rabinstein AA, Carhuapoma JR, Derdeyn CP, Dion J, Higashida RT, Hoh BL, Kirkness CJ, Naidech AM, Ogilvy CS, Patel AB, Thompson BG, Vespa P (2012) Guidelines for the management of aneurysmal subarachnoid hemorrhage: a guideline for healthcare professionals from the American Heart Association/American Stroke Association. Stroke 43:1711–1737
18. Liang N, Wang P, Wang S, Li S, Li Y, Wang J, Wang M (2014) Role of mitochondrial calcium uniporter in regulating mitochondrial fission in the cerebral cortexes of living rats. J Neural Transm 121:593–600
19. Prunell GF, Mathiesen T, Svendgaard NA (2002) A new experimental model in rats for study of the pathophysiology of subarachnoid hemorrhage. Neuroreport 13:2553–2556
20. Sun Q, Dai Y, Zhang X, Hu YC, Zhang D, Li W, Zhang XS, Zhu JH, Zhou ML, Hang CH (2013) Expression and cell distribution of myeloid differentiation primary response protein 88 in the cerebral cortex following experimental subarachnoid hemorrhage in rats: a pilot study. Brain Res 1520:134–144
21. Dai Y, Sun Q, Zhang X, Hu Y, Zhou M, Shi J (2014) Cyclosporin A ameliorates early brain injury after subarachnoid hemorrhage through inhibition of a Nur77 dependent apoptosis pathway. Brain Res 1556:67–76
22. Yamaguchi M, Zhou C, Nanda A, Zhang JH (2004) Ras protein contributes to cerebral vasospasm in a canine double-hemorrhage model. Stroke 35:1750–1755
23. Zhuang Z, Zhou ML, You WC, Zhu L, Ma CY, Sun XJ, Shi JX (2012) Hydrogen-rich saline alleviates early brain injury via reducing oxidative stress and brain edema following experimental subarachnoid hemorrhage in rabbits. BMC Neurosci 13:47
24. Cosentino K, Garcia-Saez AJ (2014) Mitochondrial alterations in apoptosis. Chem Phys Lipids 181:62–75
25. Ricci JE, Gottlieb RA, Green DR (2003) Caspase-mediated loss of mitochondrial function and generation of reactive oxygen species during apoptosis. J Cell Biol 160:65–75
26. Gaetani P, Pasqualin A, Rodriguez y Baena R, Borasio E, Marzatico F (1998) Oxidative stress in the human brain after subarachnoid hemorrhage. J Neurosurg 89:748–754
27. Nina P, Schisano G, Chiappetta F, Luisa Papa M, Maddaloni E, Brunori A, Capasso F, Corpetti MG, Demurtas F (2001) A study of blood coagulation and fibrinolytic system in spontaneous subarachnoid hemorrhage. Correlation with hunt-hess grade and outcome. Surg Neurol 55:197–203
28. Mehta A, Prabhakar M, Kumar P, Deshmukh R, Sharma PL (2013) Excitotoxicity: bridge to various triggers in neurodegenerative disorders. Eur J Pharmacol 698:6–18
29. Patron M, Raffaello A, Granatiero V, Tosatto A, Merli G, De Stefani D, Wright L, Pallafacchina G, Terrin A, Mammucari C, Rizzuto R (2013) The mitochondrial calcium uniporter (MCU): molecular identity and physiological roles. J Biol Chem 288:10750–10758
30. Ostrowski RP, Colohan AR, Zhang JH (2006) Molecular mechanisms of early brain injury after subarachnoid hemorrhage. Neurol Res 28:399–414
31. Zhang SZ, Gao Q, Cao CM, Bruce IC, Xia Q (2006) Involvement of the mitochondrial calcium uniporter in cardioprotection by ischemic preconditioning. Life Sci 78:738–745
32. Yang X, Wang B, Zeng H, Cai C, Hu Q, Cai S, Xu L, Meng X, Zou F (2014) Role of the mitochondrial Ca uniporter in Pb-induced oxidative stress in human neuroblastoma cells. Brain Res 1575:12–21. doi:10.1016/j.brainres.2014.05.032
33. Kalac P (2014) Health effects and occurrence of dietary polyamines: a review for the period 2005–mid 2013. Food Chem 161:27–39
34. Mozdzan M, Szemraj J, Rysz J, Stolarek RA, Nowak D (2006) Antioxidant activity of spermine and spermidine re-evaluated with oxidizing systems involving iron and copper ions. Int J Biochem Cell Biol 38:69–81
35. Premkumar K, Bowlus CL (2004) Ascorbic acid does not increase the oxidative stress induced by dietary iron in C3H mice. J Nutr 134:435–438
36. Salvi M, Toninello A (2004) Effects of polyamines on mitochondrial Ca(2+) transport. Biochim Biophys Acta 1661:113–124
37. Hubschmann OR, Nathanson DC (1985) The role of calcium and cellular membrane dysfunction in experimental trauma and subarachnoid hemorrhage. J Neurosurg 62:698–703
38. Wang J, Ohta S, Sakaki S, Araki N, Matsuda S, Sakanaka M (1994) Changes in Ca(++)-ATPase activity in smooth-muscle cell membranes of the canine basilar artery with experimental subarachnoid hemorrhage. J Neurosurg 80:269–275
39. Friedrich V, Flores R, Sehba FA (2012) Cell death starts early after subarachnoid hemorrhage. Neurosci Lett 512:6–11